Available online at www.sciencedirect.com
SCIENCE DIRECT®
International Journal of Heat and Mass Transfer 47 (2004) 2045–2059
International Journal of HEAT and MASS TRANSFER
www.elsevier.com/locate/ijhmt

Measurement and correlation of critical heat flux in two-phase micro-channel heat sinks

Weilin Qu, Issam Mudawar *

Boiling and Two-phase Flow Laboratory, School of Mechanical Engineering, 1288 Mechanical Engineering Building, Purdue University, West Lafayette, IN 47907-1288, USA

Received 17 October 2003; received in revised form 11 December 2003

Abstract

Critical heat flux (CHF) was measured for a water-cooled micro-channel heat sink containing 21 parallel 215×821 μm channels. Tests were performed with deionized water over a mass velocity range of 86–368 kg/m^{2}s, inlet temperatures of 30 and 60 °C, at an outlet pressure of 1.13 bar. As CHF was approached, flow instabilities induced vapor backflow into the heat sink's upstream plenum, which significantly altered the coolant temperature at the channel inlets. The backflow negated the advantages of inlet subcooling, resulting in a CHF virtually independent of inlet temperature but which increases with increasing mass velocity. Due to the vapor backflow and other unique features of parallel micro-channels, it is shown previous correlations that are quite accurate at predicting CHF for single mini-channels are unsuitable for micro-channel heat sinks. Using the new heat sink water CHF data as well as previous data for R-113 in heat sinks with multiple circular mini- and micro-channels, a new CHF correlation is proposed which shows excellent accuracy in predicting existing heat sink data.
© 2004 Elsevier Ltd. All rights reserved.

1. Introduction

The past decade has witnessed unprecedented improvements in the performance of computer processors which were brought about, for the most part, by a restless pursuit of micro-miniaturization of components in the processor itself. These advances have led to alarming increases in the amount of heat that is dissipated and has to be removed from these processors. The large increase in heat dissipation per unit surface area and per unit volume is not limited to computer processors. In fact, this trend is evident in many cutting-edge power and switching devices as well as laser diode arrays. Heat dissipation rates in these devices have already escalated to levels that can no longer be managed with conventional cooling techniques. New, more powerful cooling systems are therefore needed to both meet the challenges of emerging technologies as well as make possible further developments in these technologies that will undoubtedly bring about further increases in heat dissipation.

Several cooling schemes have been developed in recent years that capitalize upon the merits of phase change to achieve the desired cooling performance. These include pool boiling thermosyphons, channel flow boiling, jet, and sprays. Two-phase micro-channel heat sinks are a special class of channel flow boiling systems. They offer unique advantages that clearly set them apart from other high-performance cooling systems. A typical micro-channel heat sink consists of a high-conductivity slab containing multiple, parallel channels with cross-sectional dimensions of 10–1000 μm. The heat-dissipating device is attached to the planar surface of the heat sink, from which the heat is conducted to a liquid coolant that is supplied through the channels. High device heat fluxes cause the coolant to boil along the micro-channel. Two key merits of boiling in micro-channels are (1) very large convective heat transfer coefficients (i.e., low device temperatures) and (2) relatively small temperature rise along the channel compared

* Corresponding author. Tel.: +1-765-494-5705; fax: +1-765-494-0539.
E-mail address: mudawar@ecn.purdue.edu (I. Mudawar).

0017-9310/$ - see front matter © 2004 Elsevier Ltd. All rights reserved.
doi:10.1016/j.ijheatmasstransfer.2003.12.006

Nomenclature

A	parameter in empirical correlations
A_{ch}	micro-channel cross-sectional area
A_h	micro-channel heated inside area
A_t	planform area of heat sink's top surface
C	parameter in empirical correlations
C_0	void distribution parameter
c_P	specific heat at constant pressure
d	inner diameter of circular channel
d_e	heated equivalent diameter of rectangular channel
F_1 to F_4	parameters in empirical correlations
g	gravitational constant
G	mass velocity in micro-channel
h	fluid enthalpy
H_{cell}	height of heat sink unit cell
H_{ch}	height of micro-channel
h_f	enthalpy of saturated liquid
h_{fg}	latent heat of vaporization
$\Delta h_{sub,in}$	inlet subcooling
H_{w1}	thickness of plastic cover plate
H_{w2}	distance from thermocouple to micro-channel bottom wall
K	inlet subcooling parameter
K_1 to K_3	parameters in empirical correlations
k_f	thermal conductivity of liquid
k_s	thermal conductivity of copper heat sink
L	heated length of micro-channel
$\dot{m}$	total mass flow rate
M	number of data points
MAE	mean absolute error
n	parameter in empirical correlations
N	number of micro-channels in heat sink
P	pressure
P_h	inside heated perimeter of channel
$P_{p,out}$	pump exit pressure
P_R	reduced pressure in Bowring correlation
P_W	total electrical power input to heat sink's cartridge heaters
q''_{eff}	effective heat flux based on heat sink's top planform area
$q''_{eff,m}$	CHF based on heat sink's top planform area
q''_p	mean heat flux based on channel heated inside area
$q''_{p,m}$	CHF based on channel heated inside area
$q''_{p,m0}$	CHF based on channel heated inside area for zero inlet subcooling
$q''_{p,m01}$ to $q''_{p,m05}$	parameters in empirical correlations
tc1 to tc4	thermocouples
T	temperature
T_{sat}	saturation temperature
T_{tci}	thermocouple reading ($i = 1$ to 4)
$T_{w,tci}$	channel bottom wall temperature at thermocouple location
W_{cell}	width of heat sink unit cell
W_{ch}	width of micro-channel
W_w	half-width of wall separating micro-channels
We	Weber number
x_e	thermodynamic equilibrium quality
z	stream-wise location

Greek symbols

λ	characteristic wavelength
ρ	density
σ	surface tension

Subscripts

exp	experimental (measured)
f	liquid
g	vapor
in	inlet
out	outlet
m	maximum (critical heat flux)
pred	predicted
s	solid (copper heat sink)
tc*i*	thermocouple ($i = 1$ to 4)

to single-phase micro-channel cooling. Coupled with their intrinsically small thickness, these two advantages greatly reduce overall thermal resistance between the device and coolant, reduce coolant flow rate and inventory requirements, and provide a high degree of temperature uniformity along the flow direction. These attributes have made these heat sinks a prime contender for compact, lightweight cooling systems in such applications as satellites, avionics, and portable computers.

These practical merits of two-phase micro-channel heat sinks have attracted considerable attention in recent years on several issues concerning their phase change characteristics. These include boiling incipience [1,2], dominant flow patterns [3–5], hydrodynamic instability [6–9], heat transfer [10–14], and pressure drop [9,12,15–19]. The issue of critical heat flux (CHF), however, has received very limited attention, despite the great importance of this parameter to the design and safe operation of a heat sink.

CHF generally refers to the outcome of events that cause a sudden, appreciable decrease in the heat transfer coefficient for a surface on which boiling is occurring. For a heat-flux-controlled system, such as the case with most practical two-phase micro-channel heat sinks, exceeding CHF can lead to a sudden large increase in surface temperature, which, for most coolants, can lead to catastrophic system failure. The ability to determine CHF is therefore of vital importance to the safety of two-phase micro-channel heat sinks since only with such knowledge can a heat sink be designed with an acceptable margin of safety relative to maximum heat flux dissipation or minimum coolant flow rate.

Two-phase micro-channel heat sinks generally involve flow boiling in straight, constant-cross-sectional-area channels with constant mass flow rate and uniform heat distribution along the flow direction. For such systems, CHF generally commences at the channel outlet [20,21]. According to whether the bulk fluid at channel outlet is subcooled or saturated when CHF occurs, flow-boiling CHF can be classified as either *subcooled CHF* or *saturated CHF*. The two types of CHF are triggered by drastically different mechanisms.

Subcooled CHF indicates situations where the bulk fluid temperature at the channel outlet is subcooled when CHF occurs. This condition is represented by a thermodynamic equilibrium quality, which is defined as

$$x_e = \frac{h - h_f}{h_{fg}}, \tag{1}$$

that is less than zero at the outlet, $x_{e,out} < 0$. Conditions that often lead to subcooled CHF include large mass velocity, high inlet subcooling, and/or channels with a small length-to-diameter ratio. At the channel outlet, the bulk fluid remains in mostly liquid state with a large number of very small vapor bubbles confined to the heated wall. Researchers have proposed several theories to explain the trigger mechanism for subcooled CHF: intense boiling causes the bubble-liquid boundary layer to be separated from the heated wall and the resulting stagnant liquid to evaporate [22], bubble crowding within the boundary layer inhibits liquid replenishment near the surface causing the formation of an insulating vapor layer [23], and dryout of a liquid sublayer beneath large vapor bubbles causes the local wall temperature to rise appreciably [24]. Hall and Mudawar [25] provided a comprehensive review of the current state of knowledge of subcooled CHF for water flow boiling in channels, and derived a statistical correlation based on the entire world subcooled CHF database available until 1999.

Saturated CHF is encountered in situations where $x_{e,out} \geqslant 0$ when CHF occurs. Conditions that commonly lead to saturated CHF include small mass velocity, low inlet subcooling, and/or channels with a large length-to-diameter ratio. The corresponding flow pattern at the channel outlet is mostly annular with the vapor phase occupying most of the channel core while the liquid flows as a thin film along the channel wall. Dryout of the liquid film near the outlet is widely regarded as the trigger mechanism for saturated CHF [20,21]. Micro-channel heat sinks are especially prone to this type of CHF since they are used in applications demanding minimal flow rates and small coolant inventory.

As the transport process behind flow boiling CHF is extremely complex, CHF predictions rely heavily on empirical correlations that are derived from experimental CHF databases [21,25]. Available saturated CHF data for flow boiling in mini/micro-channels were compiled by the present authors and are summarized in Table 1. In this paper, mini-channels refer to channels with characteristic cross-sectional dimensions from about 1 to 3 mm, and micro-channels less than 1 mm. The database contains 438 saturated CHF data points, including 392 for water flow in single circular mini-channels ($d = 1$–3 mm), 22 for Refrigerant R-113 in single circular mini-channels ($d = 3.15$ mm), and 24 for R-113 in circular mini-($d = 2.54$ mm) and micro-channel ($d = 510$ μm) heat sinks. Sources and parameter ranges for the CHF data are also provided in Table 1. In addition to those listed in Table 1, Nariai et al. [32] and Yu et al. [33] also conducted experimental studies on saturated CHF of water in single circular mini-channels. However, their data are excluded from the database as they were not available in fully characterized tabular form. Close examination of Table 1 reveals a severe shortage of data for micro-channels, and clearly points to a need for further experimental study. With the exception of Bowers and Mudawar's work [15], all other saturated CHF data were obtained using single channels. CHF in a heat sink containing multiple parallel channels may be significantly different from that in a single channel, as boiling and two-phase flow are less stable in the former. Another aspect of the database is that all the available saturated CHF data are for circular channels, while channels in practical heat sinks are mostly rectangular because of their ease of fabrication. Finally, the majority of the saturated CHF data are for mini-channels whose inner diameters are considerably larger than those employed in micro-channel heat sinks.

The present study explores flow boiling CHF for a water-cooled two-phase micro-channel heat sink. The primary objectives of the present study are: (1) to provide new saturated CHF data for flow boiling in a heat sink containing rectangular micro-channels, (2) to assess the accuracy of previous empirical CHF correlations for both single mini-channels as well as mini/micro-channel heat sinks, and (3) to develop a new CHF correlation

Table 1
Parameter ranges of saturated CHF data for flow boiling in mini/micro-channels

Reference	No. of data	d (mm)	L/d	G (kg/m^{2}s)	P_{out} (bar)	T_{in} (°C)	$x_{e,out}$	$q''_{p,m}$ (W/cm^2)
(a) Water flow boiling in single circular mini-channels								
Lowdermilk et al. [26]	188	1.30	50.0	94.9	1.01	22.2	0.020	23.0
		2.44	250.0	30379.8	7.91	25.6	0.980	2504.8
Weatherhead [27]	6	1.14	100.0	4370.0	13.8	153.87	0.210	732.0
		1.14	100.0	5180.0	13.8	165.62	0.265	732.0
Becker [28]	82	2.40	166.7	365.0	31.0	19.33	0.207	114.0
		3.00	208.3	2725.0	71.0	83.78	0.891	513.0
Lezzi et al. [29]	68	1.00	239.0	776.0	29.4	22.9	0.660	28.5
		1.00	975.0	2738.0	72.0	288.0	0.990	236.3
Roach et al. [30]	48	1.17	110.5	246.6	3.36	48.90	0.362	86.0
		1.45	137.0	1036.9	10.42	72.50	1.182	369.8
(b) R-113 flow boiling in single circular mini-channels								
Lazarek and Black [31]	22	3.15	40.0	232.0	1.14	23.90	0.290	18.3
		3.15	40.0	503.0	4.14	94.30	0.887	33.6
(c) R-113 flow boiling in circular mini and micro-channel heat sinks								
Bowers and Mudawar [15]	24	0.51	3.94	29.8	1.06	37.26	0.581	35.54
		2.54	19.61	476.3	1.37	37.26	1.528	105.50

that is particularly suited for mini/micro-channel heat sinks.

2. Experimental apparatus

2.1. Test module

Fig. 1(a) illustrates the layered construction of the micro-channel heat sink test module. The micro-channels were cut into the 4.48 cm long and 1.0 cm wide top surface of an oxygen-free copper block. Twenty-one 215 μm wide and 821 μm deep micro-slots were machined within the 1-cm width of the top surface. Heat was supplied to the micro-channels from twelve high-power-density cartridge heaters that were inserted into bores in the underside of the copper block.

The copper bock was inserted along the central hollowed section of a thermally insulating G-7 fiberglass plastic housing. A small protruding platform around the periphery of the heat sink ensured that the top surface of the heat sink was flush with the top surface of the housing. The housing contained a deep plenum leading to another shallow plenum both upstream and downstream of the heat sink to ensure even flow distribution. A polyetherimide thermoplastic (GE Ultem 1000) cover plate was bolted atop the heat sink. Aside from forming the top surface for the individual micro-channels, this semi-transparent cover plate provided visual access to the flow boiling inside the micro-channels. After the test module was assembled, multiple layers of ceramic fiber were wrapped around the copper block to reduce heat loss to the ambient.

Four Type K thermocouples, indicated in Fig. 1(a) as tc1 to tc4 (from upstream to downstream), were inserted below the top surface of the heat sink to measure the stream-wise temperature distribution along the central plane. Error associated with the thermocouple readings was smaller than ±0.3 °C. The cartridge heaters were powered by a 0–110 VAC variac and their total electrical power input measured by a 0.5% accuracy wattmeter. Located in the deep plenums were two absolute pressure transducers and two Type-K thermocouples for inlet and outlet pressure and temperature measurements, respectively. The uncertainty for these pressure and temperature measurements was 3.5% and ±0.3 °C, respectively.

Prior to performing the CHF measurements, a series of single-phase tests were conducted within the same flow rate range. Comparison between electrical power input and the increase in water enthalpy during these single-phase tests showed heat loss was smaller than 4%. All heat flux data presented in this study were therefore based on the measured electrical power input.

2.2. Flow loop

Deionized water was supplied to the test module using the flow loop illustrated schematically in Fig. 1(b). The bulk of the water resided in a reservoir which also served as a deaeration chamber. A gear pump provided the necessary pressure rise at the module inlet over the desired range of flow rates. The water flow rate was measured by one of two rotameters that were arranged in parallel. Measurement uncertainty of the flow meters was better than 4%. Two control valves, one situated

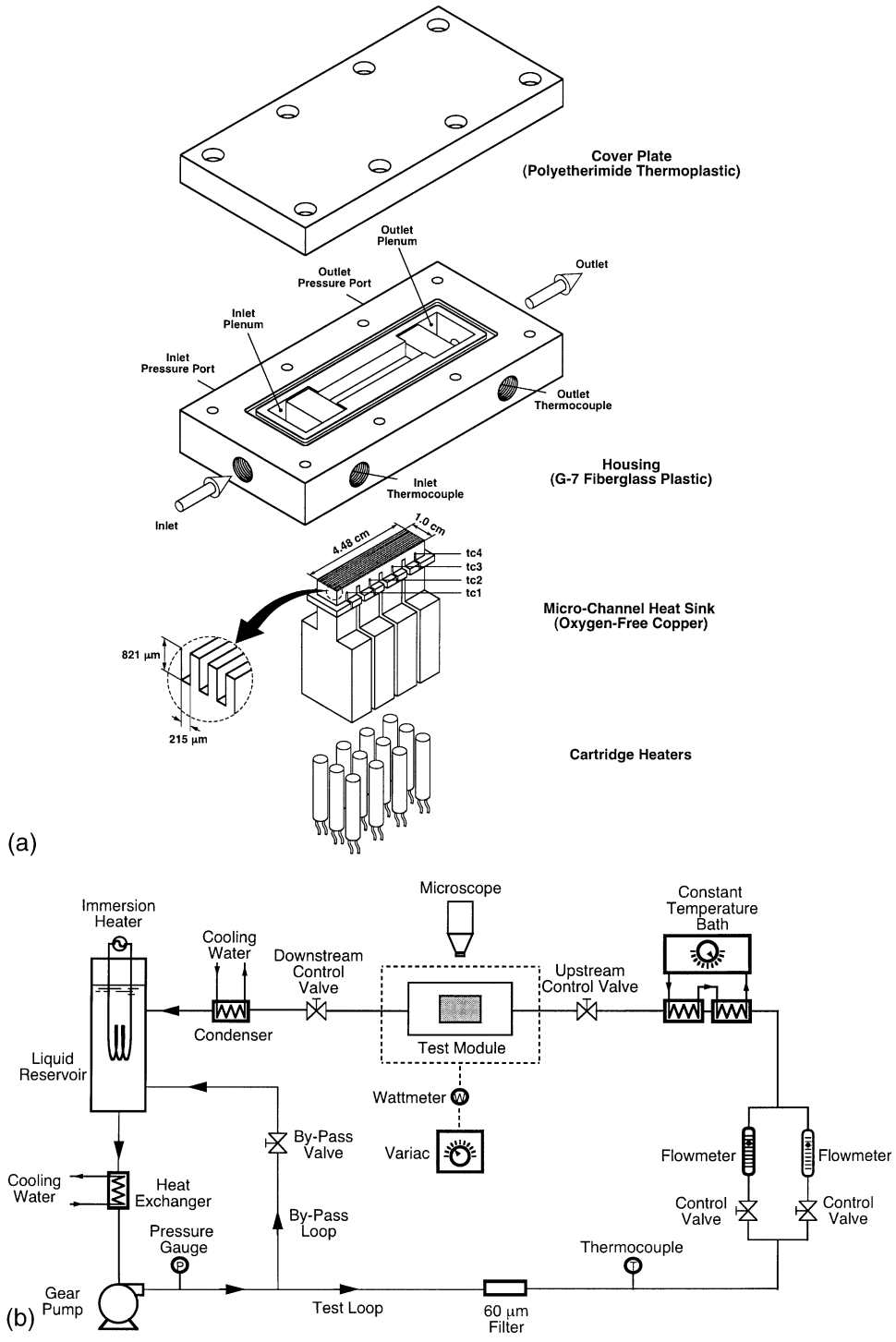

Fig. 1. (a) Test module construction and (b) schematic of flow loop.

upstream and the other downstream of module, played a vital role in the flow regulation. The downstream valve was used to regulate the heat sink's outlet pressure. Throttling the upstream valve eliminated a type of instability, *severe pressure drop oscillation*, which is caused by interaction between the two-phase flow in the parallel micro-channels and the upstream compressible volume in the loop. Another *mild parallel channel*

instability persisted in the micro-channels even with the throttling of the upstream valve. This latter instability caused random axial oscillations of the boundary between the liquid and downstream two-phase mixture, but had a relatively mild effect on heat sink pressure drop. These flow instabilities were described in a previous paper by the present authors [9], and will be addressed briefly later in this paper.

2.3. Experimental procedure

Before making any CHF measurements, the water in the reservoir was brought to a vigorous boil inside the reservoir for about one hour to purge any dissolved gases into the ambient. Subsequently, the flow loop components were adjusted to yield the desired operating conditions according to Table 2.

Using the upstream valve, the pump exit pressure, $P_{p,out}$, was elevated to about 2.0 bar to prevent the aforementioned severe pressure drop oscillation. After the flow became stable, the heater power was adjusted to a level below incipient boiling. The power was then increased in small increments and the flow loop components were continuously adjusted to maintain the desired operating conditions. Following each power increment, the heat sink was allowed sufficient time to reach steady-state, and the inlet and outlet pressures, P_{in} and P_{out}, inlet and outlet temperatures, T_{in} and T_{out}, and heat sink temperatures, T_{tc1} to T_{tc4}, were all recorded using an HP data acquisition system that was interfaced to a PC.

Each test was terminated when CHF was encountered in the micro-channel heat sink. After CHF was triggered at the channel outlet, it propagated upstream along the channel. With a short time delay, the thermocouple closest to the channel outlet (tc4) sensed a sudden unsteady temperature rise. The test was then terminated once CHF reached the location of tc4 to avoid over heating of the test module.

The water mass velocity G was determined from the measured mass flow rate, $\dot{m}$, number of micro-channels, N, and cross-sectional area, A_{ch}, of a micro-channel.

$$G = \frac{\dot{m}}{NA_{ch}}. \tag{2}$$

Two definitions are used in the present study for heat flux to the heat sink. The first is an "effective" heat flux, q''_{eff}, defined as the total electrical power input measured by the wattmeter, P_W, divided by the top planform area of the heat sink, $A_t = 1.0 \times 4.48\ \text{cm}^2$.

$$q''_{eff} = \frac{P_W}{A_t}. \tag{3}$$

The second definition is a mean heat flux averaged over the micro-channel heated inside area, q''_p, as illustrated in Fig. 2 for a heat sink unit cell containing a single micro-channel as well as surrounding solid-dimensions of the unit cell are given in Table 3. While q''_{eff} provides a global measure of the heat sink's thermal performance, q''_p is more useful when investigating empirical flow boiling CHF correlations. Referring to Fig. 2, q''_p can be related to q''_{eff} by

$$q''_p = \frac{q''_{eff} W_{cell}}{W_{ch} + 2H_{ch}}. \tag{4}$$

The CHF values reported in this study represent the highest heat flux ($q''_{eff,m}$ or $q''_{p,m}$) measured for stable flow boiling before the last power increment that precipitated the unsteady temperature rise.

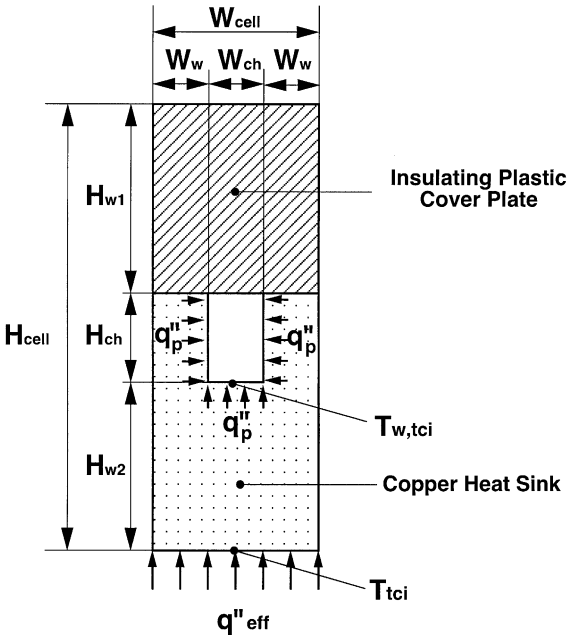

Fig. 2. Unit cell of micro-channel heat sink.

Table 2
Operating conditions for present study

Coolant	Inlet temperature, T_{in} (°C)	Mass velocity, G (kg/m^{2}s)	Outlet pressure, P_{out} (bar)	Pump exit pressure, $P_{p,out}$ (bar)
Deionized water	30.0	86–368	1.13	2.0
	60.0	86–368	1.13	2.0

Table 3
Dimensions of micro-channel heat sink unit cell

W_w (μm)	W_{ch} (μm)	H_{w1} (μm)	H_{ch} (μm)	H_{w2} (μm)
125	215	12,700	821	2354

3. Results and discussion

3.1. Boiling curve

Fig. 3(a) and (b) show typical boiling curves obtained at the four thermocouple locations for a mass velocity of 228 kg/m^{2}s and inlet temperatures of 30 and 60 °C, respectively. The effective heat flux, q''_{eff}, is plotted versus the difference between the local channel bottom wall temperature, $T_{w,tci}$, and inlet temp erature, T_{in}. Referring to Fig. 2, $T_{w,tci}$ was evaluated from q''_{eff} and thermocouple readings T_{tci} by assuming one-dimensional heat conduction between thermocouple location and channel bottom wall immediately above.

$$T_{w,tci} = T_{tci} - \frac{q''_{eff} H_{w2}}{k_s}. \quad (5)$$

The inlet temperature T_{in} was measured directly by the thermocouple located in the upstream plenum. However, as the heat flux approached CHF, the parallel-channel instability, which had been mild over a wide range of heat fluxes, became quite intense. This caused a significant amount of vapor from the micro-channels to flow backwards into the upstream plenum and mix with the incoming subcooled liquid. This was clearly manifest by upstream plenum thermocouple reading temperatures significantly higher than that of the incoming liquid, T_{in}. Under these conditions, the incoming liquid temperature is assigned the value of T_{in}. This issue will be discussed in more detail in the next section.

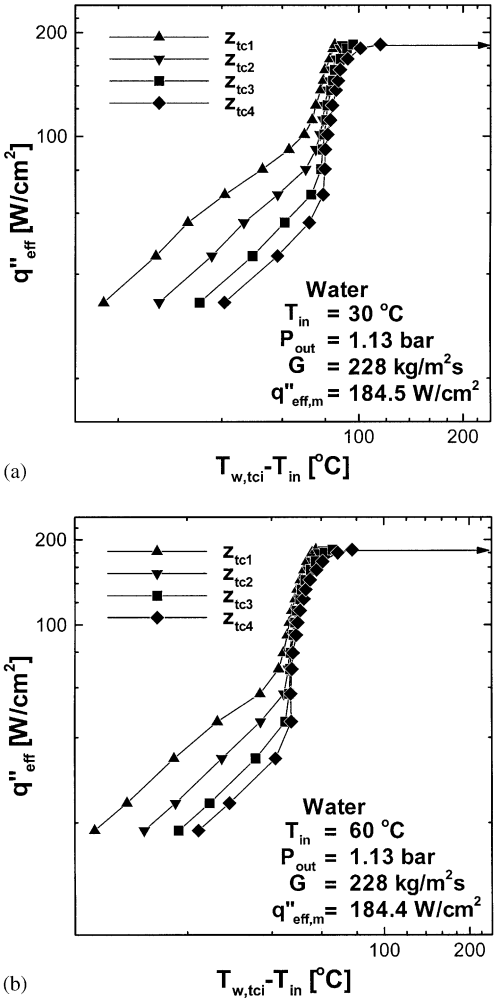

Fig. 3. Boiling curves measured at z_{tc1} to z_{tc4} for (a) $G = 228$ kg/m^{2}s and $T_{in} = 30$ °C, and (b) $G = 228$ kg/m^{2}s and $T_{in} = 60$ °C.

Fig. 3(a) and (b) show the slopes of all boiling curves are fairly constant at low heat fluxes corresponding to the single-phase liquid cooling regime. With increasing heat flux, the slope of the boiling curve begins increasing at z_{tc4}, indicating flow boiling is initiated near the outlet. Further heat flux increases cause similar slope changes for the upstream thermocouple locations in uniform succession. As the heat flux approaches CHF, the slope begins to decrease again, indicative of reduced heat transfer effectiveness, which also begins at z_{tc4} and propagates upstream at slightly higher fluxes. Eventually, CHF is detected at z_{tc4}. CHF values for the conditions given in Fig. 3(a) and (b) are $q''_{eff,m} = 184.5$ and 184.4 W/cm^2, respectively.

3.2. Hydrodynamic instability

In a previous study by the present authors [9], two types of flow instability were identified in the heat sink test module as described in the previous section. The first-severe pressure drop oscillation-was the result of interaction between the two-phase flow in the heat sink and the upstream compressible volume in the flow loop. This instability produced severe flow oscillations across the heat sink, which occurred when the control valve upstream of the module was fully open. The boiling boundary between the liquid and downstream two-phase mixture in all channels showed severe fluctuation, moving back and forth in unison between the inlet and outlet. By throttling the upstream control valve, this

severe flow oscillation was virtually eliminated, and the boiling boundary fluctuated between micro-channels in a random but mild manner. This second type of instability was classified as mild parallel channel instability, resulting from micro-channel interactions that are intrinsic to the heat sink itself.

All the present tests were therefore conducted with the upstream control valve throttled. During the tests, however, it was observed that the parallel channel instability, which was very mild over a large portion of the heat flux range, became severe as CHF was approached. Fig. 4 shows a schematic of the micro-channel inlet at these high pre-CHF heat fluxes. Vapor was observed to flow backwards from the individual micro-channels into the upstream shallow plenum, eventually forming a thick intermittent vapor layer. This layer was broken up into many small vapor bubbles, which propagated further upstream even into deep plenum, where it mixed with the incoming liquid. The upstream plenum interactions between the vapor and incoming liquid significantly altered the fluid temperature in the deep plenum. Fig. 5 shows the upstream plenum thermocouple readings are fairly constant over a broad range of heat fluxes but begin to increase significantly for the last two or three heat flux increments immediately prior to CHF. Recall that the boiling curves shown in Fig. 3(a) and (b) were referenced relative to a T_{in} value equal to the mean thermocouple readings corresponding to lower heat fluxes. These values are shown as horizontal lines in Fig. 5.

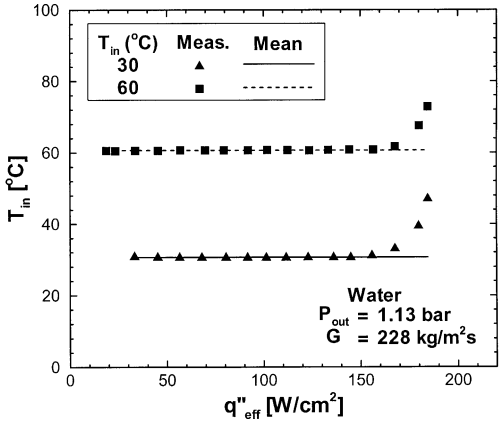

Fig. 5. Inlet temperature versus effective heat flux for $G = 228$ kg/m^{2}s and $T_{in} = 30$ and 60 °C.

3.3. CHF characteristics

The CHF data measured during the present study are given in Table 4 along with the corresponding operating conditions. Inlet temperature, T_{in}, is based on the average of measured inlet temperatures before the pre-CHF loss of subcooling depicted in Fig. 5 begins to take effect. Outlet quality, $x_{e,out}$, is evaluated using Eq. (1), where the outlet fluid enthalpy, h_{out}, is determined by applying an energy balance for the entire heat sink.

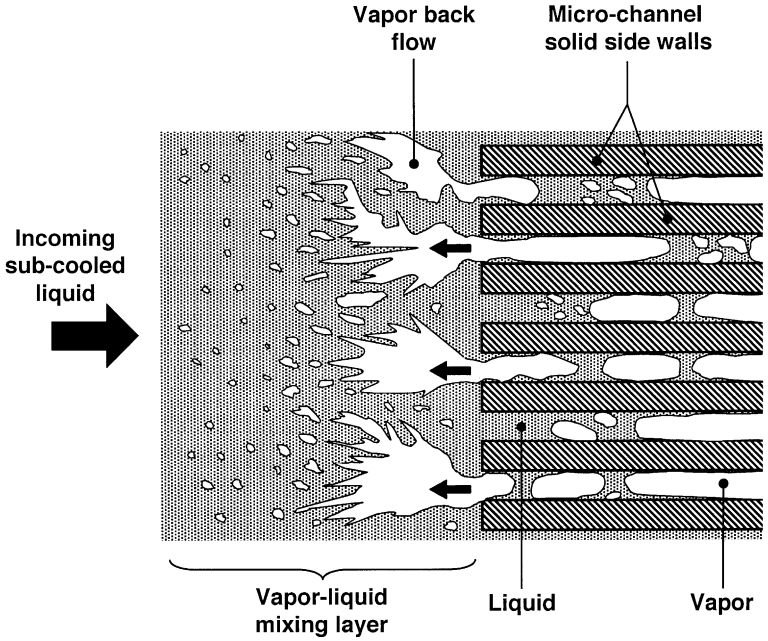

Fig. 4. Schematic representation of observed vapor backflow as heat flux approaches CHF.

Table 4
Present CHF data for water in rectangular micro-channel heat sink

T_{in} (°C)	G (kg/m^{2}s)	P_{in} (bar)	P_{out} (bar)	$x_{e,out}$	$q''_{eff,m}$ (W/cm^2)	$q''_{p,m}$ (W/cm^2)
32.16	85.9	1.213	1.131	0.524	107.64	26.91
30.66	124.2	1.231	1.127	0.398	126.48	31.62
31.66	159.2	1.271	1.133	0.376	154.94	38.74
31.46	194.5	1.285	1.129	0.310	164.93	41.24
30.65	228.0	1.310	1.135	0.288	184.48	46.13
30.60	263.2	1.331	1.130	0.250	193.64	48.42
30.54	299.5	1.309	1.123	0.214	200.00	50.01
30.65	336.1	1.331	1.132	0.178	201.66	50.42
30.63	368.4	1.324	1.139	0.172	216.76	54.20
59.00	85.9	1.223	1.131	0.562	105.66	26.42
60.69	124.2	1.249	1.135	0.434	121.69	30.43
60.50	159.2	1.310	1.141	0.424	153.21	38.31
58.96	194.5	1.314	1.131	0.361	164.60	41.16
60.69	228.0	1.366	1.140	0.344	184.43	46.12
59.34	263.2	1.375	1.132	0.295	189.59	47.41
60.88	299.5	1.398	1.135	0.283	207.33	51.84
59.94	336.1	1.393	1.143	0.233	201.59	50.41
59.63	368.4	1.375	1.133	0.214	207.85	51.97

$$h_{out} = h_{in} + \frac{q''_{eff} A_t}{\dot{m}}. \quad (6)$$

The thermophysical properties used in Eq. (1) were based on the outlet pressure P_{out}. Table 4 shows $x_{e,out}$ values at CHF are all positive, indicating saturated CHF conditions. In addition, increasing mass velocity G from 85.9 to 368.4 kg/m^{2}s decreases $x_{e,out}$ from 0.524 to 0.172 for $T_{in} = 30$ °C and 0.562 to 0.214 for $T_{in} = 60$ °C.

Fig. 6 shows CHF increases monotonically with increasing G for both inlet temperatures. However, what is quite surprising is inlet temperature, T_{in}, has virtually no effect on CHF.

Interestingly, these CHF trends relative to mass velocity G and inlet temperature T_{in} mirror those of Bowers and Mudawar for Refrigerant R-113 in circular mini and micro-channel heat sinks [15]. While the trend of increasing CHF with increasing G is quite common, the lack of inlet temperature effect on CHF seems to be unique to two-phase mini/micro-channel heat sinks, not single micro/mini-channels. A key difference between heat sinks and single channels is the aforementioned amplification of parallel channel instability prior to CHF. As discussed earlier, this amplification causes back flow of vapor into the upstream plenum, which results in strong mixing of the vapor with the incoming liquid. Regardless how subcooled the incoming liquid is, the mixing action appears to increase the temperature of the liquid close to the local saturation temperature as it approaches the channel inlet.

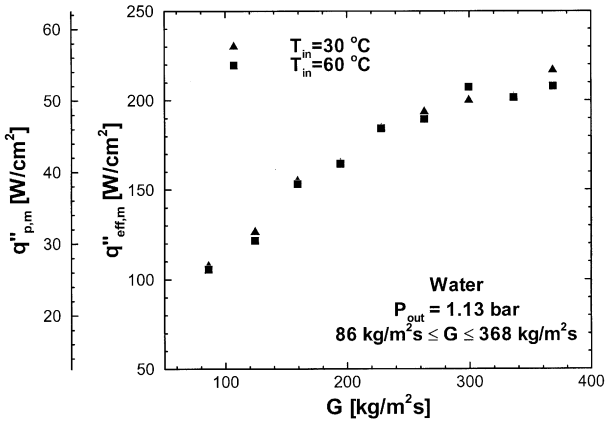

Fig. 6. Variation of CHF with mass velocity.

3.4. Assessment of previous CHF correlations

In this section, the applicability of previous CHF correlations to predicting saturated flow boiling CHF in single mini-channels as well as in mini/micro-channel heat sinks is examined through comparison of correlation predictions with experimental CHF data.

Summarized in Table 5 are the Bowring [34,35] and the Katto and Ohno correlations [36], which are the most popular among numerous correlations developed for saturated flow boiling CHF in single (isolated) circular channels [20]. These two correlations are first compared with saturated CHF data for water and R-113 in single circular mini-channels that were compiled by the present authors and presented earlier in Table 1. Fig. 7(a) shows the Bowring correlation agrees quite well with the CHF data in the low CHF range, but shows poor predictive capability in the high CHF range. The mean absolute error (MAE) for this correlation, which is defined as

$$\mathrm{MAE} = \frac{1}{M}\sum \frac{|q''_{p,m,\mathrm{pred}} - q''_{p,m,\mathrm{exp}}|}{q''_{p,m,\mathrm{exp}}} \times 100\%, \tag{7}$$

is 28.3% for a total of $M = 414$ data point. Fig. 7(b) shows the Katto and Ohno correlation yields superior predictions over the entire heat flux range. The MAE for this correlation is 17.3% with most of the data points falling within a ±40% error band.

Fig. 8(a) and (b) compare the predictions of the Bowring and the Katto and Ohno correlations with the present CHF data of water in the micro-channel heat sink. As the present channel shape is rectangular, a heated equivalent diameter, d_e, defined as [37]

$$d_e = \frac{4A_{ch}}{P_h} = \frac{4A_{ch}}{W_{ch} + 2H_{ch}}, \tag{8}$$

Table 5
Correlations for saturated flow boiling CHF in single circular channels

Reference	
[34,35]	$q''_{p,m} = \frac{A - 0.25 d G \Delta h_{\mathrm{sub,in}}}{C+L}$
	$\Delta h_{\mathrm{sub,in}} = h_f - h_{\mathrm{in}}$; $A = \frac{2.317(dGh_{fg}/4)F_1}{1.0+0.0143F_2 d^{0.5} G}$; $C = \frac{0.077F_3 dG}{1.0+0.347F_4(G/1356)^n}$
	$n = 2.0 - 0.5P_R$; $P_R = 0.145P_{\mathrm{out}}$; P_{out} in MPa
	$F_1 = \frac{1}{1.917}\left\{P_R^{18.942}\exp[20.89(1.0-P_R)] + 0.917\right\}$; $F_2 = \frac{1.309F_1}{P_R^{1.316}\exp[2.444(1.0-P_R)]+0.309}$
	$F_3 = \frac{1}{1.667}\left\{P_R^{17.023}\exp[16.658(1.0-P_R)] + 0.667\right\}$; $F_4 = F_3 P_R^{1.649}$
[36]	$q''_{p,m} = q''_{p,m0}\left(1.0 + K\frac{\Delta h_{\mathrm{sub,in}}}{h_{fg}}\right)$
	$q''_{p,m01} = C(Gh_{fg})We^{-0.043}\frac{1}{L/d}$
	$q''_{p,m02} = 0.1(Gh_{fg})\left(\frac{\rho_g}{\rho_f}\right)^{0.133}We^{-1/3}\frac{1}{1+0.0031L/d}$
	$q''_{p,m03} = 0.098(Gh_{fg})\left(\frac{\rho_g}{\rho_f}\right)^{0.133}We^{-0.433}\frac{(L/d)^{0.27}}{1+0.0031L/d}$
	$q_{p,m04} = 0.0384(Gh_{fg})\left(\frac{\rho_g}{\rho_f}\right)^{0.6}We^{-0.173}\frac{1}{1+0.28We^{0.233}(L/d)}$
	$q''_{p,m05} = 0.234(Gh_{fg})\left(\frac{\rho_g}{\rho_f}\right)^{0.513}We^{-0.433}\frac{(L/d)^{0.27}}{1+0.0031L/d}$
	$We = \frac{G^2 L}{\sigma\rho_f}$; $C = 0.25$ for $\frac{L}{d} < 50$; $C = 0.25 + 0.0009\left(\frac{L}{d} - 50\right)$ for $50 \leqslant \frac{L}{d} \leqslant 150$
	$C = 0.34$ for $\frac{L}{d} > 150$
	$K_1 = \frac{0.261}{CWe^{-0.043}}$; $K_2 = \frac{0.833(0.0124+d/L)}{(\rho_g/\rho_f)^{0.133}We^{-1/3}}$; $K_3 = \frac{1.12(1.52We^{-0.233}+d/L)}{(\rho_g/\rho_f)^{0.6}We^{-0.173}}$
	For $\frac{\rho_g}{\rho_f} < 0.15$:
	When $q''_{p,m01} < q''_{p,m02}$, $q''_{p,m0} = q''_{p,m01}$
	When $q''_{p,m01} > q''_{p,m02}$, if $q''_{p,m02} < q''_{p,m03}$, $q''_{p,m0} = q''_{p,m02}$; if $q''_{p,m02} > q''_{p,m03}$, $q''_{p,m0} = q''_{p,m03}$
	When $K_1 > K_2$, $K = K_1$; when $K_1 < K_2$, $K = K_2$
	For $\frac{\rho_g}{\rho_f} > 0.15$:
	When $q''_{p,m01} < q''_{p,m05}$, $q''_{p,m0} = q''_{p,m01}$
	When $q''_{p,m01} > q''_{p,m05}$, if $q''_{p,m05} > q''_{p,m04}$, $q''_{p,m0} = q''_{p,m05}$; if $q''_{p,m05} < q''_{p,m04}$, $q''_{p,m0} = q''_{p,m04}$
	When $K_1 > K_2$, $K = K_1$; when $K_1 < K_2$, if $K_2 < K_3$, $K = K_2$; if $K_2 > K_3$, $K = K_3$

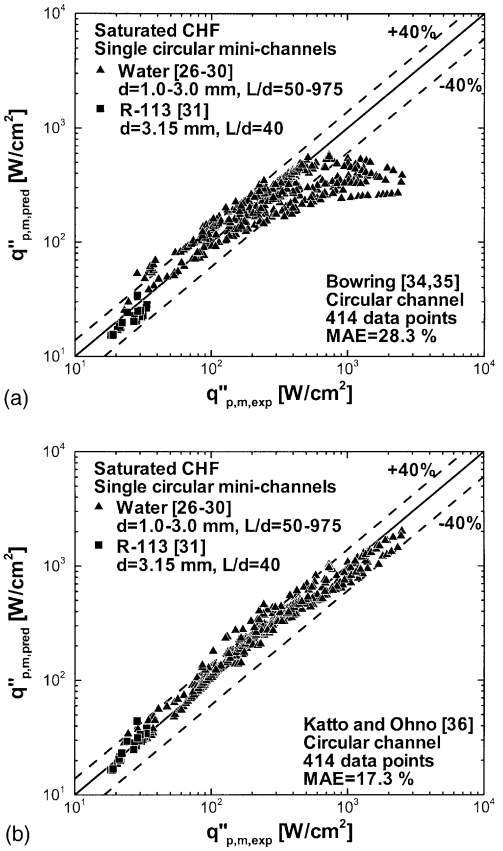

Fig. 7. Comparison of CHF data for water and R-113 in single circular mini-channels with predictions of circular channel correlations of (a) Bowring [34,35] and (b) Katto and Ohno [36].

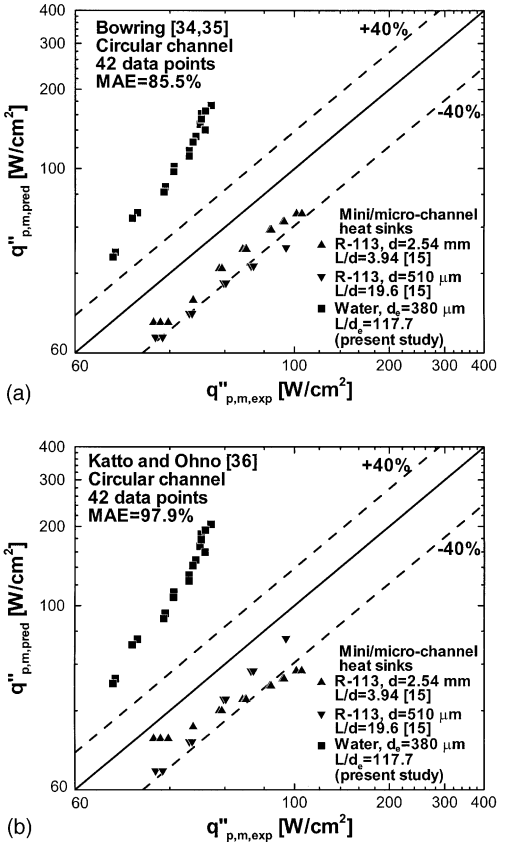

Fig. 8. Comparison of CHF data for water and R-113 in mini/micro-channel heat sinks with predictions of circular channel correlations of (a) Bowring [34,35] and (b) Katto and Ohno [36].

is employed to replace channel diameter d in the two correlations. Fig. 8(a) and (b) show both correlations overpredict the present CHF data by a large margin. This large deviation may be attributed to the aforementioned pre-CHF amplification of the parallel channel instability as well as the rectangular shape of the present micro-channels. Also shown in Fig. 8(a) and (b) are comparisons of the predictions of the two correlations with the saturated CHF data for R-113 in mini/micro-channel heat sinks measured earlier by Bowers and Mudawar [15]. The correlations generally underpredict the R-113 data as well, even though many data points are located within a ±40% error band.

Published work on saturated CHF in rectangular channels is far more limited than that in circular. Table 6 summarizes four correlations that were developed from saturated CHF in single rectangular channels. Comparisons between correlation predictions and the present CHF data in the rectangular micro-channel heat sink are shown in Fig. 9(a)–(d). Among the four correlations tested, the correlation by Sudo et al. [39] shows the best agreement (MAE of 19.8%) with the data. However, a close examination of the same correlation, Table 6, shows it relates CHF to mass velocity and thermophysical properties of the coolant, but none of the channel geometrical parameters. Since saturated flow boiling CHF is affected by both channel length L and heated equivalent diameter d_e [20], the seemingly accurate predictions of this correlation are not sufficient to justify its use for heat sink design.

The above assessment of prior correlations points to the need for developing a new correlation that is specifically tailored to mini/micro-channel heat sinks that contain multiple, parallel channels.

3.5. New CHF correlation

A new CHF correlation is developed based on the present CHF data for water in the rectangular micro-channel heat sink, as well as Bowers and Mudawar's CHF data for R-113 in the circular mini/micro-channel heat sinks. Drastic differences between the

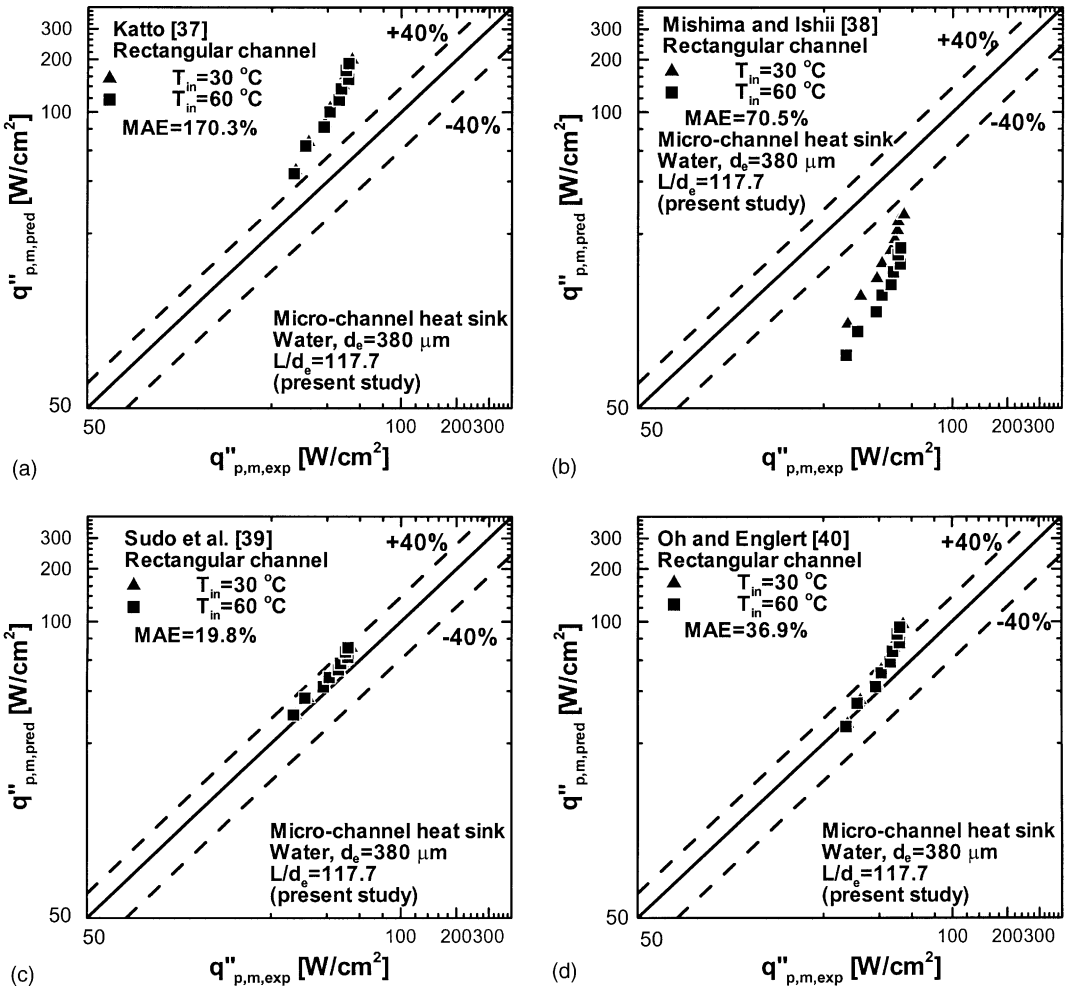

Fig. 9. Comparison of CHF data for water in present rectangular micro-channel heat sink with predictions of rectangular channel correlations of (a) Katto [37], (b) Mishima and Ishii [38], (c) Sudo et al. [39], and (d) Oh and Englert [40].

thermophysical properties of water and R-113, Table 7, as well as the differences in both channel shape, channel diameter, and L/d ratio are all especially useful in developing a correlation with a broad application appeal based on these two CHF databases. The new CHF correlation adopts the functional form of the Katto and Ohno correlation [36]. As shown in Table 5, the Katto and Ohno correlation for zero inlet subcooling is given by

$$\frac{q''_{p,m0}}{Gh_{\mathrm{fg}}} = f\left\{\frac{\rho_{\mathrm{g}}}{\rho_{\mathrm{f}}}, We, \frac{L}{d_{\mathrm{e}}}\right\}, \tag{9}$$

where We is the Weber number based on the channel heated length L,

$$We = \frac{G^2 L}{\sigma \rho_{\mathrm{f}}}. \tag{10}$$

Assuming CHF increases linearly with increasing inlet subcooling yields

$$q''_{p,m} = q''_{p,m0}\left(1 + K\frac{\Delta h_{\mathrm{sub,in}}}{h_{\mathrm{fg}}}\right). \tag{11}$$

Since CHF for both mini/micro-channel heat sink databases shows no dependence on inlet subcooling, these databases are correlated according to Eq. (9), i.e. without the subcooling multiplier.

$$\frac{q''_{p,m}}{Gh_{\mathrm{fg}}} = 33.43\left(\frac{\rho_{\mathrm{g}}}{\rho_{\mathrm{f}}}\right)^{1.11} We^{-0.21}\left(\frac{L}{d_{\mathrm{e}}}\right)^{-0.36}, \tag{12}$$

where d_{e} should be set equal to d for circular mini/micro-channel heat sinks.

Fig. 10 compares the predictions of this new CHF correlation with the flow boiling CHF data for both water in the present rectangular micro-channel heat sink and R-113 in the Bowers and Mudawar circular mini/micro-channel heat sinks. The overall MAE of 4%

Table 6
Correlations for saturated flow boiling CHF in single rectangular channels

Reference	
[37]	$q''_{p,m} = q''_{p,m0}\left(1.0 + K\frac{\Delta h_{\text{sub,in}}}{h_{\text{fg}}}\right)$
	$q''_{p,m01} = 0.25(Gh_{\text{fg}})\frac{1}{L/d_{\text{e}}}$; $q''_{p,m02} = C(Gh_{\text{fg}})We^{-0.043}\frac{1}{L/d_{\text{e}}}$
	$q''_{p,m03} = 0.15(Gh_{\text{fg}})\left(\frac{\rho_{\text{g}}}{\rho_{\text{f}}}\right)^{0.133}We^{-1/3}\frac{1}{1+0.0077L/d_{\text{e}}}$
	$q''_{p,m04} = 0.26(Gh_{\text{fg}})\left(\frac{\rho_{\text{g}}}{\rho_{\text{f}}}\right)^{0.133}We^{-0.433}\frac{(L/d_{\text{e}})^{0.171}}{1+0.0077L/d_{\text{e}}}$
	$C = 0.25$ for $\frac{L}{d_{\text{e}}} < 50$; $C = 0.34$ for $\frac{L}{d_{\text{e}}} > 50$
	$K_1 = 1$; $K_2 = \frac{0.261}{CWe^{-0.043}}$; $K_3 = \frac{0.556(0.0308+d_{\text{e}}/L)}{(\rho_{\text{g}}/\rho_{\text{f}})^{0.133}We^{-1/3}}$
	When $q''_{p,m01} < q''_{p,m02}$, $q''_{p,m0} = q''_{p,m01}$, $K = K_1$
	When $q''_{p,m01} > q''_{p,m02}$, if $q''_{p,m02} < q''_{p,m03}$, $q''_{p,m0} = q''_{p,m02}$, $K = K_2$
	if $q''_{m02} > q''_{m03}$, if $q''_{p,m03} < q''_{p,m04}$, $q''_{p,m0} = q''_{p,m03}$, $K = K_3$
	if $q''_{p,m03} > q''_{p,m04}$, $q''_{p,m0} = q''_{p,m04}$
[38]	$q''_{p,m} = \frac{A_{\text{ch}}}{A_{\text{h}}}h_{\text{fg}}\left[\frac{G\Delta h_{\text{sub,in}}}{h_{\text{fg}}} + \left(\frac{1}{C_0} - 0.11\right)\sqrt{\rho_{\text{g}}g(\rho_{\text{f}} - \rho_{\text{g}})d_{\text{e}}}\right]$
	$C_0 = 1.35 - 0.35\sqrt{\frac{\rho_{\text{g}}}{\rho_{\text{f}}}}$
[39]	$q''_{p,m} = 0.005h_{\text{fg}}G^{0.611}[\lambda\rho_{\text{g}}g(\rho_{\text{f}} - \rho_{\text{g}})]^{0.195}$
	$\lambda = \sqrt{\frac{\sigma}{(\rho_{\text{f}} - \rho_{\text{g}})g}}$
[40]	$q''_{p,m} = \frac{A_{\text{ch}}}{A_{\text{h}}}h_{\text{fg}}\left[0.458G\left(1.0 - \frac{\Delta h_{\text{sub,in}}}{h_{\text{fg}}}\right) + 2.412\sqrt{\lambda\rho_{\text{g}}g(\rho_{\text{f}} - \rho_{\text{g}})}\right]$

Table 7
Thermophysical properties of saturated water and saturated R-113 at one atmosphere

Properties	Water	R-113
Saturation temperature, T_{sat} (°C)	100.0	47.6
Density of liquid, ρ_{f} (kg/m^3)	957.9	1507.3
Density of vapor, ρ_{g} (kg/m^3)	0.60	7.48
Latent heat of vaporization, h_{fg} (kJ/kg)	2257	158
Surface tension, σ (N/m)	0.0589	0.0147
Liquid specific heat at constant pressure, c_{p} (kJ/kg K)	4.217	0.922
Thermal conductivity of liquid, k_{f} (W/m K)	0.68	0.07

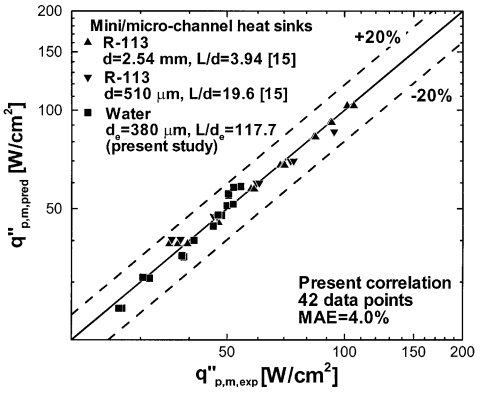

Fig. 10. Comparison of CHF data for water and R-113 in mini/micro-channel heat sinks with predictions of present correlation.

clearly demonstrates its excellent predictive capability for different fluids, circumferential heating conditions, channel geometries, channel sizes, and length-to-diameter ratios.

4. Conclusions

In this study, experiments were performed to measure CHF for water flow boiling in a rectangular micro-channel heat sink. Previous empirical CHF correlations were examined for suitability to predicting saturated CHF in single mini-channels as well as in mini/micro-channel heat sinks. A new empirical correlation was developed for CHF in two-phase mini/micro-channel heat sinks. Key findings from the study are as follows:

(1) The mild parallel channel instability intrinsic to micro-channel heat sink with multiple, parallel channels is greatly amplified as heat flux approaches CHF. This causes the vapor to flow backwards into

the inlet plenum, mix with the incoming liquid, and increase the liquid temperature to the local saturation temperature as the liquid enters the micro-channels.

(2) CHF in mini/micro-channel heat sinks increases with increasing mass velocity but, because of the loss of subcooling due to the backward vapor flow, CHF is virtually independent of inlet temperature. This is a fundamental departure of mini/micro-channel heat sink behavior from that of single mini-channels.

(3) The Katto and Ohno correlation [36] is fairly accurate at predicting saturated CHF in single circular mini-channels.

(4) Two widely used circular channel CHF correlations and four rectangular channel CHF correlations were tested relative to the present rectangular micro-channel heat sink data. A correlation by Sudo et al. [39] for CHF in single rectangular channels showed the best agreement with the experimental data. However, this correlation is not recommended for heat sink design because of its failure to account for channel length or diameter.

(5) A new empirical correlation is proposed based on experimental flow boiling CHF data for water and R-113 in multiple-channel mini/micro-channel heat sinks. The overall MAE of this correlation of 4% demonstrates its excellent predictive capability for different fluids, circumferential heating conditions, channel geometries, channel sizes, and length-to-diameter ratios.

Acknowledgements

The authors are grateful for the support of the Office of Basic Energy Sciences of the US Department of Energy (Award no. DE-FG02-93ER14394 A7).

References

[1] J.E. Kennedy, G.M. Roach Jr., M.F. Dowling, S.I. Abdel-Khalik, S.M. Ghiaasiaan, S.M. Jeter, Z.H. Quershi, The onset of flow instability in uniformly heated horizontal microchannels, J. Heat Transfer 122 (2000) 118–125.

[2] W. Qu, I. Mudawar, Prediction and measurement of incipient boiling heat flux in micro-channel heat sinks, Int. J. Heat Mass Transfer 45 (2002) 3933–3945.

[3] L. Zhang, J.M. Koo, L. Jiang, S.S. Banerjee, M. Ashegi, K.E. Goodson, J.G. Santiago, T.W. Kenny, Measurement and modeling of two-phase flow in microchannels with nearly-constant heat flux boundary conditions, in: A. Lee et al. (Eds.), Micro-Electro-Mechanical Systems (MEMS)—2000, ASME, Orlando, FL, 2000, MEMS-vol. 2, pp. 129–135.

[4] L. Jiang, M. Wong, Y. Zohar, Forced convection boiling in a microchannel heat sink, J. Microelectromech. Syst. 10 (2001) 80–87.

[5] W. Qu, I. Mudawar, Transport phenomena in two-phase micro-channel heat sinks, in: Y. Bayazitoglu, H.S. Cameron, (Eds.), Proceedings of the ASME Heat Transfer Division – 2002, ASME, New York, NY 2002, HTD-vol. 372–7, pp. 135–147.

[6] S.G. Kandlikar, M.E. Steinke, S. Tian, and L.A. Campbell, High-speed photographic observation of flow boiling of water in parallel mini-channels, in: Proceedings of 35th National Heat Transfer Conference, ASME, Anaheim, CA, 2001, pp. 675–684.

[7] G. Hetsroni, A. Mosyak, Z. Segal, G. Ziskind, A uniform temperature heat sink for cooling of electronic devices, Int. J. Heat Mass Transfer 45 (2002) 3275–3286.

[8] H.Y. Wu, P. Cheng, Visualization and measurements of periodic boiling in silicon microchannels, Int. J. Heat Mass Transfer 46 (2003) 2603–2614.

[9] W. Qu, I. Mudawar, Measurement and prediction of pressure drop in two-phase micro-channel heat sinks, Int. J. Heat Mass Transfer 46 (2003) 2737–2753.

[10] X.F. Peng, B.X. Wang, Forced convection and flow boiling heat transfer for liquid flowing through microchannels, Int. J. Heat Mass Transfer 36 (1993) 3421–3427.

[11] T.S. Ravigururajan, Impact of channel geometry on two-phase flow heat transfer characteristics of refrigerants in microchannel heat exchangers, J. Heat Transfer 120 (1998) 485–491.

[12] G.R. Warrier, V.K. Dhir, L.A. Momoda, Heat transfer and pressure drop in narrow rectangular channel, Exp. Thermal Fluid Sci. 26 (2002) 53–64.

[13] W. Qu, I. Mudawar, Flow boiling heat transfer in two-phase micro-channel heat sinks—I. Experimental investigation and assessment of correlation methods, Int. J. Heat Mass Transfer 46 (2003) 2755–2771.

[14] W. Qu, I. Mudawar, Flow boiling heat transfer in two-phase micro-channel heat sinks—II. Annular two-phase flow model, Int. J. Heat Mass Transfer 46 (2003) 2773–2784.

[15] M.B. Bowers, I. Mudawar, High flux boiling in low flow rate, low pressure drop mini-channel and micro-channel heat sinks, Int. J. Heat Mass Transfer 37 (1994) 321–332.

[16] M.B. Bowers, I. Mudawar, Two-phase electronic cooling using mini-channel and micro-channel heat sinks: part 1-Design criteria and heat diffusion constraints, J. Electron. Packaging 116 (1994) 290–297.

[17] M.B. Bowers, I. Mudawar, Two-phase electronic cooling using mini-channel and micro-channel heat sinks: part 2-Flow rate and pressure drop constraints, J. Electron. Packaging 116 (1994) 298–305.

[18] T.N. Tran, M.C. Chyu, M.W. Wambsganss, D.M. France, Two-phase pressure drop of refrigerants during flow boiling in small channels: an experimental investigation and correlation development, Int. J. Multiphase Flow 26 (2000) 1739–1754.

[19] H.J. Lee, S.Y. Lee, Heat transfer correlation for boiling flows in small rectangular horizontal channels with low aspect ratios, Int. J. Multiphase Flow 27 (2001) 2043–2062.

[20] J.G. Collier, J.R. Thome, Convective Boiling and Condensation, third ed., Oxford University Press, Oxford, 1994.

[21] D.D. Hall, I. Mudawar, Critical heat flux (CHF) for water flow in tubes—I. Compilation and assessment of world CHF data, Int. J. Heat Mass Transfer 43 (2000) 2573–2604.

[22] S.S. Kutateladze, A.I. Leont'ev, Some applications of the asymptotic theory of the turbulent boundary layer, in: Proceedings of the Third International Heat Transfer Conference, American Institute of Chemical Engineers, New York, 1966, vol. 3, pp. 1–6.
[23] J. Weisman, B.S. Pei, Prediction of critical heat flux in flow boiling at low qualities, Int. J. Heat Mass Transfer 26 (1983) 1463–1477.
[24] C.H. Lee, I. Mudawar, A mechanistic critical heat flux model for subcooled flow boiling based on local bulk flow conditions, Int. J. Multiphase Flow 14 (1988) 711–728.
[25] D.D. Hall, I. Mudawar, Critical heat flux (CHF) for water flow in tubes – II. Subcooled CHF correlations, Int. J. Heat Mass Transfer 43 (2000) 2605–2640.
[26] W.H. Lowdermilk, C.D. Lanzo, B.L. Siegel, Investigation of boiling burnout and flow stability for water flowing in tubes, NACA TN 4382, National Advisory Committee for Aeronautics, 1958.
[27] R.J. Weatherhead, Heat transfer, flow instability, and critical heat flux for water in a small tube at 200 psia, ANL-6715, Argonne national Laboratory, 1963.
[28] K.M. Becker, Burnout measurements in vertical round tubes, effect of diameter, AE-TPM-RL-1260, Aktiebolaget Atomenergi, 1970.
[29] A.M. Lezzi, A. Niro, G.P. Beretta, Experimental data of CHF for forced convection water boiling in long horizontal capillary tubes, in: G.F. Hewitt (Ed.), Heat Transfer 1994: Proceedings of the Tenth Internal Heat Transfer Conference, Institution of Chemical Engineers, Rugby, United Kingdom, 1994, vol. 7, pp. 491–496.
[30] G.M. Roach Jr., S.I. Abdel-Khalik, S.M. Ghiaasiaan, M.F. Dowling, S.M. Jeter, Low-flow critical heat flux in heated microchannels, Nucl. Sci. Eng. 131 (1999) 411–425.
[31] G.M. Lazarek, S.H. Black, Evaporative heat transfer, pressure drop and critical heat flux in a small vertical tube with R-113, Int. J. Heat Mass Transfer 25 (1982) 945–960.
[32] H. Nariai, F. Inasaka, K. Uehara, Critical heat flux in narrow tubes with uniform heating, Heat Transfer—Jap. Res. 18 (1989) 21–30.
[33] W. Yu, D.M. France, M.W. Wambsganss, J.R. Hull, Two-phase pressure drop, boiling heat transfer, and critical heat flux to water in a small-diameter horizontal tube, Int. J. Multiphase Flow 28 (2002) 927–941.
[34] R.W. Bowring, A simple but accurate round tube uniform heat flux, dryout correlation over the pressure range 0.7-17 MN/m^2 (100–2500 psia), AEEW-R 789, United Kingdom Atomic Energy Authority, 1972.
[35] N.E. Todreas, M.S. Kazimi, Nuclear Systems I, Hemisphere Press, New York, 1990.
[36] Y. Katto, H. Ohno, An improved version of the generalized correlation of critical heat flux for the forced convective boiling in uniformly heated vertical tubes, Int. J. Heat Mass Transfer 27 (1984) 1641–1648.
[37] Y. Katto, General features of CHF of forced convection boiling in uniformly heated rectangular channels, Int. J. Heat Mass Transfer 24 (1981) 1413–1419.
[38] K. Mishima, M. Ishii, Critical heat flux experiments under low flow conditions in a vertical annulus, ANL-82-6, NUREG/CR-2647, 1982.
[39] Y. Sudo, K. Miyata, H. Ikawa, M. Kaminaga, M. Ohkawara, Experimental study of differences in DNB heat flux between upflow and downflow in vertical rectangular channel, J. Nucl. Sci. Technol. 22 (1985) 604–618.
[40] C.H. Oh, S.B. Englert, Critical heat flux for low flow boiling in vertical uniformly heated thin rectangular channels, Int. J. Heat Mass Transfer 36 (1993) 325–335.